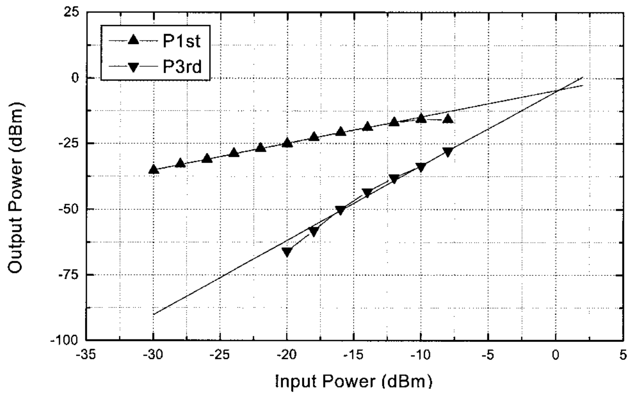

Figure 5 Measurement of IIP3 of the CMOS micromixer

RF–IF isolation is better than 24 dB for RF power below a gain-compressed point. Finally, a two-tone intermodulation measurement is performed, and the results are shown in Figure 5. $IIP_3 = 0$ dBm is obtained from the figure.

4. CONCLUSION

Gilbert cell variant topology is demonstrated in a double-balanced mixer. With a single-ended IF output measurement, a conversion loss of 4.7 dB is achieved. It is found that the linearity of this mixer is very good: the $P_{1\text{ dB}}$ is -10 dBm and IIP_3 is 0 dBm.

REFERENCES

1. B. Gilbert, The MICROMIXER: A highly linear variant of the Gilbert mixer using a bisymmetric Class-AB input stage, IEEE J Solid-State Circuits 32 (1997), 1412–1423.
2. J. Durec and E. Main, A linear class AB single-ended to differential transconverter suitable for RF circuits, IEEE MTT-S Digest, 1996, pp. 1071–1074.
3. L.A. MacEachern and T. Manku, A charge-injection method for Gilbert cell biasing, Elect Comput Eng, 1998, IEEE Canadian Conf, May 1998, pp. 365–368.

A TIME-DOMAIN BEAM-PROPAGATION METHOD FOR ANALYZING PULSED OPTICAL BEAMS IN SECOND-ORDER NONLINEAR WAVEGUIDES

Husain M. Masoudi[1]
[1] Optical Device Simulation Group
Department of Electrical Engineering
King Fahd University of Petroleum and Minerals
Dhahran 31261, Saudi Arabia

Received 1 September 2000

ABSTRACT: *The linear time-domain beam propagation method (TD–BPM) has been extended to model the propagation of pulsed optical beams in second-order nonlinear optical material of integrated waveguides. The coupled nonlinear wave equations have been derived and discretized using the explicit finite-difference method. The nonlinear TD–BPM method developed in the present work is very efficient, and is simple to implement.* © 2001 John Wiley & Sons, Inc. Microwave Opt Technol Lett 28: 253–257, 2001.

Key words: *beam propagation; optical beams; nonlinear waveguides*

1. INTRODUCTION

In the past three decades, the second-order nonlinear optical phenomenon of $\chi^{(2)}$ played a very important role in many optical applications. It was used predominantly in frequency conversion such as second-harmonic generation, parametric amplification, sum-frequency generation, and difference-frequency generation [1–4]. Most of the research focused on efficient techniques to convert to other harmonics, and recently on other effects like nonlinear phase shift to the fundamental beam [5]. At low conversion, and off phase matching between the fundamental and the second harmonic, the nonlinear phase shift behaves similar to the Kerr effect of $\chi^{(3)}$ [5]. Lately, this nonlinear phase shift process has received much attention experimentally and theoretically to achieve all-optical switching in integrated optics [6]. In order to fully understand the complicated behavior taking place in second-order nonlinear interaction, accurate and efficient techniques must be available to model such devices. On the other hand, modeling nonlinear integrated optical waveguides is difficult using analytical techniques like the coupled-mode theory, and can be more difficult if the integrated optical circuits contain multiple waveguides that have geometrical and/or material changes in all three spatial directions. Other numerical techniques like the beam-propagation method (BPM) and the finite-difference time-domain (FDTD) method are more suited for such problems. Both of these techniques were used to model, *in the CW domain*, optical waveguides that contain second-order nonlinear effects [7–10]. In principle, the FDTD in [9–10] should be able to model pulsed optical beams in $\chi^{(2)}$ material; however, the approximation involved showed that it is limited in its present form. The CW version reported showed limitations on the input power and the overall stability of the algorithm. In addition, the FDTD requires enormous computer resources, even for analyzing simple 2-D optical waveguides [11–12]. Recently, the beam-propagation method (BPM) was extended, using the explicit finite-difference technique, to the time domain to model pulsed optical beams [11–12]. The accuracy of the TD–BPM was tested rigorously in three different problems of homogeneous medium, metallic and dielectric waveguides. In addition to its validity in homogeneous and metallic problems, it was also concluded that the technique is well suited to study pulsed optical beams in dielectric waveguides over long distances with high efficiency.

In this work, we extend the TD–BPM [11–12] to model pulsed optical beams in the presence of second-order nonlinear effects. The parabolic coupled nonlinear wave equations for the fundamental and the second-harmonic fields were derived in the time domain. All features of time and three-dimensional spatial variations were retained, and the fundamental pulse is allowed to deplete. Previous attempts to model pulsed optical beams in $\chi^{(2)}$ material involved a 1-D (plane-wave) approximation, with many time derivative terms removed to simplify the analysis [1–4, 13–14]. In this work, the explicit finite-difference (EFD) technique was used to discretize the coupled system of nonlinear equations. The EFD method is well known for its simplicity, efficiency, and is also suited for parallel computer implementations that can model large 3-D optical devices [15]. For simplicity, we refer to the new nonlinear time-domain BPM method as TD–BPM–SHG. Finally, the method is applied to model waveguides containing second-order nonlinear effects under different conditions, and the results are analyzed.

2. NUMERICAL METHOD

We start with the wave equation for the propagation of an electric field E of a given polarization in a material with a refractive index n and a homogeneous second-order nonlinear susceptibility $\chi^{(2)}$:

$$\nabla^2 E = \mu_0 \varepsilon_0 n^2 \frac{\partial^2 E}{\partial t^2} + \mu_0 \varepsilon_0 \frac{\partial^2 P}{\partial t^2} \tag{1}$$

where the nonlinear polarization $P = \chi^{(2)} EE$ and ∇^2 is the three-dimensional (x, y, z) Laplacian. Here, it is assumed that the fields are linearly polarized, and the vector nature of the fields can be ignored. This is a good first approximation for the paraxial problems of the type considered here for which the BPM is appropriate [8]. Consider the propagation of three pulsed optical fields of different central frequencies ω_1, ω_2, and ω_3, while extracting the fast oscillating carriers and reference phases in the direction of propagation z. The fields can be expressed as

$$E^{\omega_1}(x, y, z, t) = \frac{1}{2}[\phi^{\omega_1}(x, y, z, t) e^{j(\omega_1 t - k_1 n_1 z)} + \text{c.c.}] \tag{2a}$$

$$E^{\omega_2}(x, y, z, t) = \frac{1}{2}[\phi^{\omega_2}(x, y, z, t) e^{j(\omega_2 t - k_2 n_2 z)} + \text{c.c.}] \tag{2b}$$

$$E^{\omega_3}(x, y, z, t) = \frac{1}{2}[\phi^{\omega_3}(x, y, z, t) e^{j(\omega_3 t - k_3 n_3 z)} + \text{c.c.}] \tag{2c}$$

where n_1, n_2, and n_3 are reference refractive indexes, and k_1, k_2, and k_3 are the free-space wavenumbers at the three frequencies ω_1, ω_2 and ω_3, respectively. $\omega_3 = \omega_1 + \omega_2$, and c.c. is the complex conjugate of the expression preceding it. The above describes the general behavior of sum-frequency, difference-frequency generation, and parametric amplification. For simplicity, we restrict the analysis in this work to second-harmonic generation, and assume $\omega_1 = \omega_2 = \omega$ (fundamental) and $\omega_3 = \omega_1 + \omega_2 = 2\omega$ (second harmonic); then $k_1 = k_2 = k_3/2 = k_0 = 2\pi/\lambda_f$, and λ_f is the fundamental field wavelength. General frequency conversion techniques can be derived similarly. Thus, Eqs. (2a) and (2b) become identical, and therefore we are left with the analysis of two nonlinear equations. Upon inserting (2) in (1) and setting the coefficients of $e^{j\omega t}$ and $e^{j2\omega t}$ equal to zero, we may write the two equations under the parabolic approximation, after neglecting only terms containing the second derivative with respect to z, as

$$\begin{aligned} 2jk_0 n_{0f} \frac{\partial \phi^f}{\partial z} &= \nabla_\perp^2 \phi^f + k_0^2 \left(n_f^2 - n_{0f}^2\right) \phi^f - \frac{n_f^2}{c^2}\left[\frac{\partial^2 \phi^f}{\partial t^2} + 2j\omega \frac{\partial \phi^f}{\partial t}\right] \\ &\quad - \frac{\chi^{(2)}}{c^2}\left\{2\frac{\partial \phi^{f*}}{\partial t}\frac{\partial \phi^s}{\partial t} + 2j\omega\phi^{f*}\frac{\partial \phi^s}{\partial t} + 2j\omega\phi^s \frac{\partial \phi^{f*}}{\partial t}\right. \\ &\quad \left. + \phi^{f*}\frac{\partial^2 \phi^s}{\partial t^2} + \phi^s \frac{\partial^2 \phi^{f*}}{\partial t^2} - \omega^2 \phi^{f*}\phi^s\right\} e^{-j\Delta k z} \end{aligned} \tag{3a}$$

$$\begin{aligned} 4jk_0 n_{0s} \frac{\partial \phi^s}{\partial z} &= \nabla_\perp^2 \phi^s + 4k_0^2 (n_s^2 - n_{0s}^2)\phi^s - \frac{n_s^2}{c^2}\left[\frac{\partial^2 \phi^s}{\partial t^2} + 4j\omega \frac{\partial \phi^s}{\partial t}\right] \\ &\quad - \frac{\chi^{(2)}}{c^2}\left\{\frac{\partial \phi^f}{\partial t}\frac{\partial \phi^f}{\partial t} + 4j\omega\phi^f \frac{\partial \phi^f}{\partial t}\right. \\ &\quad \left. + \phi^f \frac{\partial^2 \phi^f}{\partial t^2} - 2\omega^2 \phi^f \phi^f\right\} e^{j\Delta k z} \end{aligned} \tag{3b}$$

where $\nabla_\perp^2 = (\partial^2/\partial x^2) + (\partial^2/\partial y^2)$ is the transverse Laplacian and $\Delta k = 2k_0(n_{0s} - n_{0f})$. The $\phi(x, y, z, t)$ are the parabolic fields which are paraxial approximations to the $\Phi(x, y, z, t)$ (the Helmholtz fields). $\phi^{\omega_3}(x, y, z, t) = \phi^s(x, y, z, t)$, $\phi^{\omega_1}(x, y, z, t) = \phi^{\omega_2}(x, y, z, t) = \phi^f(x, y, z, t)$, c is the speed of light in free space, and $\chi^{(2)} = \chi^{(2)}(2\omega; \omega, \omega) = \chi^{(2)}(\omega; 2\omega, -\omega)/2$ [5, 6]. In this analysis, the source field ϕ^f is allowed to deplete during propagation. $n_{0f} = n_1 = n_2$ and $n_{0s} = n_3$ are reference refractive indexes that can be chosen as the effective refractive indexes of the guided modes [8, 11]. n_f and n_s are the refractive indexes at the fundamental and the second harmonic, and "*" means the complex conjugate of the field. For convenience, throughout the rest of this work, subscripts or superscripts for both f and s are related to the fundamental wave and the second-harmonic wave respectively. In addition to the full time variation, Eq. (3) describes fully the three-dimensional interaction of the two optical pulses at the two different frequencies. Equation (3a) describes the propagation of the fundamental pulsed beam, and Eq. (3b) describes the propagation of the second-harmonic pulsed beam. It can be seen that the two equations are coupled, nonlinear, and nontrivial to solve. One may notice that the linear TD−BPM [11, 12] equation can be extracted from Eq. (3) if $\chi^{(2)}$ is set to zero, and if the field is time independent, then Eq. (3) solves the classical CW BPM−SHG [7, 8].

The substitution of a moving time coordinate $\tau = t - z/v_g$ with arbitrary v_g while using the central finite-difference approximations [7, 8, 16]

$$\frac{\partial \phi(x, y, z, \tau)}{\partial z} = \frac{1}{2\Delta z}(\phi(x, y, z + \Delta z, \tau) - \phi(x, y, z - \Delta z, \tau)) \tag{4a}$$

$$\frac{\partial \phi(x, y, z, t)}{\partial \tau} = \frac{1}{2\Delta \tau}(\phi(x, y, z, \tau + \Delta \tau) - \phi(x, y, z, \tau - \Delta \tau)) \tag{4b}$$

$$\frac{\partial^2 \phi(x, y, z, \tau)}{\partial \tau^2} = \frac{1}{\Delta \tau^2}(\phi(x, y, z, \tau + \Delta \tau) + \phi(x, y, z, \tau - \Delta \tau) - 2\phi(x, y, z, \tau)) \tag{4c}$$

$$\begin{aligned} \nabla_\perp^2 \phi(x, y, z, \tau) &= \frac{1}{\Delta x^2}(\phi(x + \Delta x, y, z, \tau) + \phi(x - \Delta x, y, z, \tau)) \\ &\quad + \frac{1}{\Delta y^2}(\phi(x, y + \Delta y, z, \tau) + \phi(x, y - \Delta y, z, \tau)) \end{aligned}$$

$$- 2\left(\frac{1}{\Delta x^2} + \frac{1}{\Delta y^2}\right)\phi(x, y, z, \tau) \quad (4d)$$

to replace the partial derivatives in Eq. (3) leads to the second-order accurate explicit finite-difference time-domain BPM for second-harmonic generation (TD−BPM−SHG):

$$\phi^f_{i,p,m}(z + \Delta z) = \phi^f_{i,p,m}(z + \Delta z) + \mathbf{M}^f_{i,p,m}\phi^f_{i,p,m}(z) + \mathbf{L}^f_\chi \phi^{f*}_{i,p,m}(z)\phi^s_{i,p,m}(z)e^{-j\Delta k z} \quad (5a)$$

$$\phi^s_{i,p,m}(z + \Delta z) = \phi^s_{i,p,m}(z + \Delta z) + \mathbf{M}^s_{i,p,m}\phi^s_{i,p,m}(z) + \mathbf{L}^s_\chi \phi^f_{i,p,m}(z)\phi^z_{i,p,m}(z)e^{j\Delta k z}. \quad (5b)$$

i, p, and m represent the discretization of x, y, and τ, respectively. $\mathbf{M}^f_{i,p,m}$ and $\mathbf{M}^s_{i,p,m}$ are very sparse complex matrices containing the linear coefficients of the fundamental and SH fields, respectively. $\mathbf{L}^f_\chi$ and $\mathbf{L}^s_\chi$ are also very sparse complex matrices containing the nonlinear coefficients of the fundamental and SH fields, respectively. The discretized equations (5) are very similar to the classical CW equations [7, 8], but with an additional transverse variable τ. The explicit propagation of the optical field using the TD−BPM−SHG is quite simple where it involves a multiplication of the input fields with very sparse matrices, which makes the method very efficient and very well suited for parallel-computer implementations [7, 8, 15]. Two numerical windows are used to advance the fields in Eq. (5): one for the fundamental pulse, and the other for the second-harmonic pulse. It has been noticed that the TD−BPM−SHG algorithm in (5) is stable for a propagational step Δz very close to the value of the linear TD−BPM counterpart [11, 12]. Examination of the differences between the two algorithms shows that the nonlinear term in (5) has very little effect on the stability of the method because practical values of $\chi^{(2)}$ are on the order of 10^{-12} m/V.

3. RESULTS AND DISCUSSIONS

In this section, the TD−BPM−SHG algorithm is implemented and used to simulate the propagation of a temporal pulse inside optical dielectric waveguides in the presence of a second-order nonlinear effect. The method was examined using different initial conditions, and the results are analyzed. The symmetric dielectric slab waveguide in Figure 1 has been used for the analysis with a fundamental carrier optical wavelength of $\lambda_f = 0.6$ μm, a slab width $d = 1$ μm, a nonlinear coefficient $\chi^{(2)} = 10$ pm/V, $n_{gf} = 1.52$, and $n_{\text{sub}} = n_{\text{cla}} = 1.50$. These parameters are chosen as typical practical parameters of nonlinear material [2, 3]. The nonlinear coefficient is restricted only in the guiding region of the waveguide. The slab waveguide was excited, at $z = 0$, with a pulsed first guided mode of the fundamental field, and a zero field was assumed for the SH. A Gaussian temporal pulse of the form $\phi^f(x, z = 0, \tau) = \phi^f_0(x)e^{-\tau^2/\sigma^2}$ is assumed, where σ scales the initial pulse. Figure 2 shows the normalized plot of the input of an initial pulse width of 100 fs.

3.1. Nonphase-Matched Case. The first simulation involves a nonphase-matched example in which the modes' effective indexes of the guided modes at the carrier frequencies are *not* equal. For the parameters of the waveguides of Figure 1 and at the fundamental wavelength, the waveguide supports a single mode with an effective index of 1.511313. On the other hand, when the guided layer refractive index at the second harmonic wavelength $n_{gs} = 1.53$, then the waveguide supports three guided modes, with the effective refractive index of the first guided mode equal to 1.525804. Figure 3 shows the normalized intensities of the fundamental and the second harmonic as a function of the propagational direction z. The plot shows that the two pulses exchange energy with a damped oscillatory behavior [2, 3]. This is a known behavior for the propagation of a nonphase-matched pulse in $\chi^{(2)}$ material, where the oscillation is due to the nonphase matching and the damping is due to the group-velocity mismatch (GVM) between the fundamental and the SH pulses [2, 3].

3.2. Phase-Matched Case. In this simulation, the refractive index of the guiding layer at the second-harmonic frequency is changed to $n_{gs} = 1.514741$ such that the two modes' effective indexes of the first guided modes at the carrier frequencies are equal. Figure 4 shows the normalized intensities of the fundamental and the second harmonic versus the longitudinal distance z for different input's amplitudes. Due to the phase-matching effect, a smooth exchange of energy between the two pulses is demonstrated. It is clear from Figure 4 that, as the input power increases, the exchange of energy takes place in shorter distances due to the dependence of $\chi^{(2)}$ on input power [4, 5, 8]. Figure 5 shows the normalized spatial field plots at the peak of the pulses for the fundamental and the SH at various distances (every 300 μm) inside the wave-

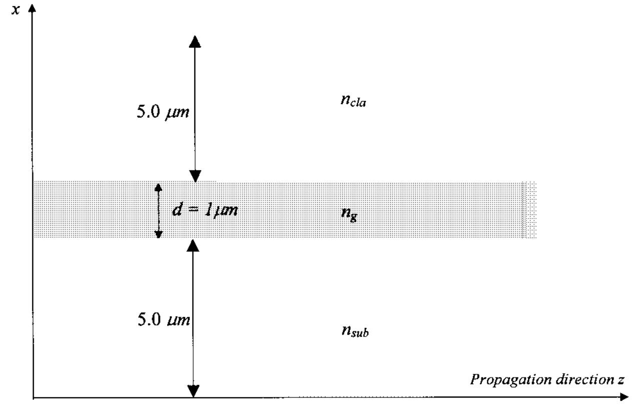

Figure 1 Two-dimensional slab dielectric waveguide used in the analysis. $n_{gf} = 1.52$, $n_{\text{sub}} = n_{\text{cla}} = 1.50$, and $\lambda_f = 0.6$ μm

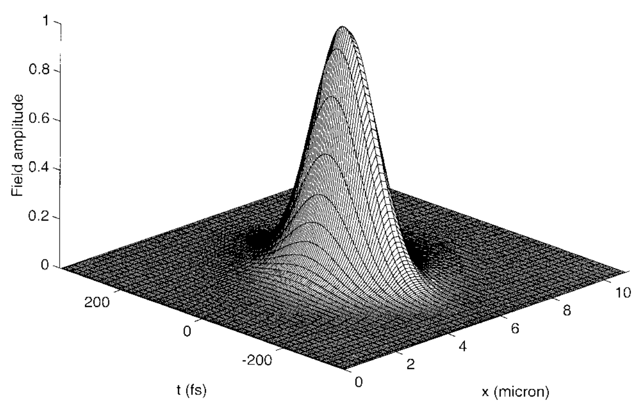

Figure 2 Three-dimensional plot of the input field used in the analysis, which consists of a pulsed first guided mode with an initial pulse width of 100 fs

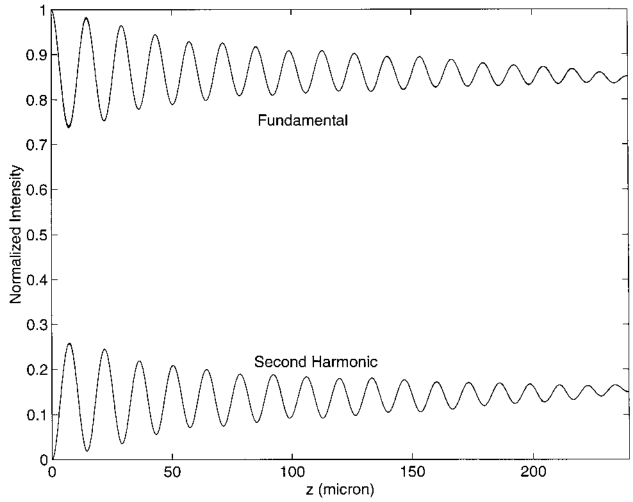

Figure 3 Normalized intensities of both the fundamental and the second-harmonic fields as a function of the propagational direction inside the nonphase-matched optical waveguide. The input field was excited with an amplitude of 5×10^9 and a pulsed first guided mode with an initial pulse width of 100 fs

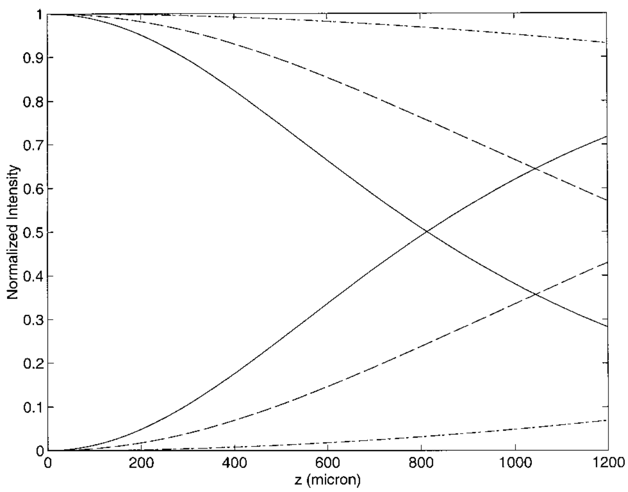

Figure 4 Normalized intensities of both the fundamental and the second-harmonic fields as a function of the propagational direction inside the phase-matched optical waveguide for different input amplitudes (dashed–dotted is for 1×10^7, dashed is for 3×10^7, and solid is for 5×10^7) and with an initial pulse width of 150 fs. Curves starting from 1 belong to the *fundamental field*, and curves starting from 0 belong to the SH field

guide. In Figure 5(a), the fields are the input (the largest) and the fundamental fields at every 300 μm in a decreasing order of amplitude, while in Figure 5(c), the fields are for the SH in an increasing order of amplitude (the largest being at $z = 1200$ μm). Figure 5(b), (d) shows the normalized fields of Figure 5(a), (c), respectively. For comparison, the normalized analytical guided mode field at the second-harmonic wavelength is also added in Figure 5(d). All of the fields in Figure 5(b), (d) are indistinguishable from each other. It is to be concluded from Figure 5(c), (d) that strong excitation of the first guided mode at the SH is taking place due to the phase-matching condition [7, 8]. Figure 6 shows the normalized pulse widths for both the fundamental and the second harmonic as a function of propagation distance. The normalization is with respect to the fundamental initial pulse width. Pulse widths of both the fundamental and the SH are broadened due to the GVM between the two pulses [1–4]. In the same figure, the ratio between the pulse width at the SH and the pulse width at the fundamental also has been included. The curve shows that the pulse width of the SH starts at $\approx 1/\sqrt{2}$, decreasing to $\approx 1/\sqrt{3}$ of the fundamental pulse width.

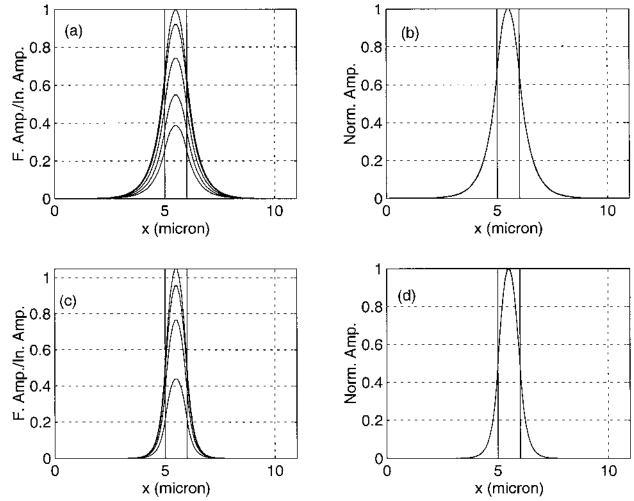

Figure 5 Propagation of the spatial fields inside the phase-matched slab waveguide using the TD–BPM–SHG. The fields shown are the input and the propagated fields every 300 μm. All parameters are the same as those of Figure 4, with an input amplitude equal to 5×10^7. The vertical lines show the position of the slab waveguide. (a) Fundamental field normalized to the input amplitude. (b) Same as in (a) normalized to the maximum. (c) SH field normalized to the input amplitude. (d) Same as in (b) normalized to the maximum, in addition to the normalized analytical guided mode field. See text for other details.

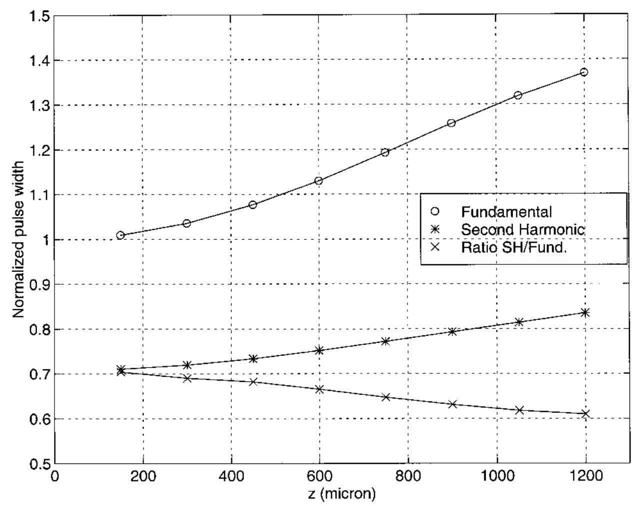

Figure 6 Fundamental and SH pulse widths as a function of propagation for the phase-matched waveguide. Pulse widths are units of initial pulse width of the fundamental. All parameters are the same as in Figure 5

Finally, throughout the previous analysis, the following simulation parameters were used: $\Delta x = 0.1$ μm, $\Delta\tau = 2$ fs, and $\Delta z = 0.06$ μm. The efficiency of the TD–BPM–SHG is quite remarkable, with a speed under 0.08 s/propagational step Δz for each simulation of the phase-matched case. This is measured on an average 600 MHz Pentium III PC, which means that the entire simulation takes about 25 min to complete.

4. CONCLUSION

A new technique for modeling pulsed optical beams in dielectric waveguides containing second-order nonlinear effects has been proposed and implemented. The technique is called the time-domain beam propagation method for second-harmonic generation (TD–BPM–SHG), which is an extension of the linear TD–BPM. It involves solving the coupled parabolic nonlinear equations using the explicit finite-difference technique, where all spatial and time variations were retained in the analysis. The technique was also applied to model pulsed optical beams in a dielectric waveguide containing second-order nonlinear effects. It is concluded that the method is very efficient and simple to implement. The TD–BPM–SHG is well suited for the study of the unidirectional propagation of compact temporal pulses over long distances in a guided-wave environment. In addition, the method should find application in the study of spatio–temporal optical solitons in media with quadratic nonlinearity [17].

ACKNOWLEDGMENT

The support of King Fahd University of Petroleum and Minerals, Dhahran, Saudi Arabia, is gratefully acknowledged.

REFERENCES

1. P.P. Ho, D. Ji, Q.Z. Wang, and R.R. Alfano, Temporal behavior of cross-phase-modulated second-harmonic generation of ultrashort laser pulses in nonlinear-optical media, J Opt Soc Amer B 7 (1990), 276–284.
2. E. Sidick, A. Knoesen, and A. Dienes, Ultrashort-pulse second-harmonic generation in quasi-phase-matched dispersive media, Opt Lett 19 (1994), 226–268.
3. E. Sidick, A. Knosen, and A. Dienes, Ultrashort-pulse second-harmonic generation in optimized nonlinear polymer thin film structures, Int J Nonlinear Opt Phys 3 (1994), 543–563.
4. E. Sidick, A. Knosen, and A. Dienes, Ultrashort-pulse second-harmonic generation. I. Transform-limited fundamental pulses, J Opt Soc Amer B 12 (1995), 1704–1712.
5. R. DeSalvo, D.J. Hagan, M. Sheikh-Bahae, G. Stegeman, and E.W. Van Stryland, Self-focusing and self-defocusing by cascaded second-order effects in KTP, Opt Lett 17 (1992), 28–30.
6. C.N. Ironside, J.S. Aitchison, and J.M. Arnold, An all-optical switch employing the cascaded second-order nonlinearity effect, IEEE J Quantum Electron 29 (1993), 2650–2654.
7. H.M. Masoudi and J.M. Arnold, Parallel beam propagation method for the analysis of second harmonic generation, IEEE Photon Technol Lett 7 (1995), 400–402.
8. H.M. Masoudi and J.M. Arnold, Modelling second-order nonlinear effects in optical waveguides using a parallel-processing beam propagation method, IEEE J Quantum Electron 31 (1995), 2107–2113.
9. M.A. AlSunaidi, H.M. Masoudi, and J.M. Arnold, A time-domain algorithm for the analysis of second harmonic generation in nonlinear optical structures, IEEE Photon Technol Lett 12 (2000), 395–397.
10. K.M. Furati, M.A. AlSunaidi, and H.M. Masoudi, An explicit finite-difference scheme for wave propagation in nonlinear optical structures, Appl Math Lett (2000).
11. H.M. Masoudi, M.A. AlSunaidi, and J.M. Arnold, Time-domain finite-difference beam propagation method, IEEE Photon Technol Lett 9 (1999), 1274–1276.
12. H.M. Masoudi, M.A. AlSunaidi, and J.M. Arnold, Efficient time-domain beam propagation method for modeling integrated optical devices, J Lightwave Technol (submitted, 2000).
13. N.C. Kothari and X. Carlotti, Transient second-harmonic generation: Influence of effective group-velocity dispersion, J Opt Soc Am B 5 (1988), 756–764.
14. P.G.M. Bakker, P.G. Planken, and H.G. Muller, Numerical calculation of optical frequency-conversion processes: A new approach, J Opt Soc Amer B 6 (1989), 1665–1672.
15. H.M. Masoudi and J.M. Arnold, Parallel three-dimensional finite-difference beam propagation methods, Int J Numer Modeling 8 (1995), 95–107.
16. Y. Chung and N. Dagli, Analysis of Z-invariant and Z-variant semiconductor rib waveguides by explicit finite difference beam propagation method with nonuniform mesh configuration, IEEE J Quantum Electron 27 (1991), 2296–2305.
17. D. Mihalache, D. Mazilu, B. Malomed, and L. Torner, Asymmetric spatio-temporal optical solitons in media with quadratic nonlinearity, Opt Commun 152 (1998), 365–370.

THE EFFECT OF GROUND VIAS ON CHANGING SIGNAL LAYERS IN A MULTILAYERED PCB

Brock J. LaMeres[1] and T. S. Kalkur[1]
[1] Department of Electrical and Computer Engineering
University of Colorado
Colorado Springs, Colorado 80933-7150

Received 30 August 2000

ABSTRACT: *This paper describes the effect of ground vias on signal integrity when a signal changes layers and passes through multiple ground planes in a printed circuit board. An equivalent circuit is given that models the return current path when a signal passes through multiple ground planes that are not connected nearby the signal via. The effect is seen as a region of higher impedance than expected on the destination signal layer. Time-domain reflectometry measurements are taken on an actual printed circuit board that exhibits this behavior. The empirical measurements are compared to SPICE simulations of the equivalent circuit to verify the accuracy of the model.* © 2001 John Wiley & Sons, Inc. Microwave Opt Technol Lett 28: 257–260, 2001.

Key words: *multilayered circuits; packaging; interconnects; PC boards*

I. INTRODUCTION

In a multilayered printed circuit board (PCB), microstrip and strip-line transmissions lines frequently need to be able to change signal layers [1]. In most cases, this involves passing through multiple ground planes. When this occurs, the ground return current must also change the layer upon which it returns to the source driving the signal. If the return current does not maintain a constant physical relationship to the signal, the signal may become distorted when it reaches the signal layer to which it is changing. The negative impact of this phenomenon can be avoided by "tacking" the ground planes of a PCB together with vias in the regions where the transmission lines change signal layers. By connecting the ground planes together near the signal vias, the return current is able to maintain its relationship to the forward traveling signal and avoid distortion. Figure 1 shows a cross section